Trends in weather parameters at Australian Antarctic bases

Timothy Cowan and Ian Simmonds
School of Earth Sciences
The University of Melbourne
Victoria, Australia, 3010
Email: simmonds@unimelb.edu.au

Climate conditions over coastal East Antarctica are being been explored using long time series of surface weather data from Australian manned weather stations, updating the work of Russell-Head and Simmonds (1993). The data used consist of 3 hourly observations (with some gaps) at Casey (1960-2002), Davis (1957-2002), and Mawson (1954-2002). The trends in the seasonal and annual means are presented in Table 1. It shows that no significant seasonal temperature trends are observed at any station over the periods. By contrast, significant annual mean pressure reductions are observed at each station (1% confidence level), with the largest occurring at Casey (1.61 hPa decade^{-1}). This station shows significant reductions in every season. The annual mean wind speed Casey and Davis show significant positive trends (0.30 and 0.28 ms^{-1} decade $^{-1}$, respectively), and the upward seasonal tendencies are significant at at least the 5% level for all but Casey in summer. By contrast, none of the weak increases at Mawson can be said to be above the noise level. These trends are consistent with those seen in the Southern Annular Mode (Thompson *et al*. 2000).

Parameter	Station	Summer	Autumn	Winter	Spring	Annual
Surface pressure	Casey	**-1.79**	**-1.41**	**-1.50**	**-1.14**	**-1.61**
	Davis	*-1.02*	*-0.93*	**-1.24**	-0.64	**-0.96**
	Mawson	**-0.84**	-0.49	*-0.74*	-0.24	**-0.59**
Surface temperature	Casey	-0.11	0.01	0.36	0.10	0.02
	Davis	0.04	-0.09	0.15	0.20	0.03
	Mawson	-0.08	-0.20	0.03	-0.04	-0.10
Surface wind speed	Casey	0.15	**0.44**	**0.30**	**0.42**	**0.30**
	Davis	**0.29**	**0.27**	*0.21*	*0.26*	**0.28**
	Mawson	0.17	0.11	0.12	0.08	0.06

Table 1: Mean seasonal and annual trends in surface pressure (hPa decade^{-1}), surface temperature (^{o}C decade^{-1}), and surface wind speed (ms^{-1} decade^{-1}) at the three coastal Australian Antarctic stations. Trends which differ significantly from zero at the 1% and 5% confidence levels are indicated in **bold** and *italics*, respectively.

Another key aspect of variability identified in the high southern latitudes is the semiannual oscillation (SAO) in surface pressure (Simmonds 2003). Across the Southern Hemisphere in recent times this feature was strong during the 1970s, weakened towards the early 1980s and remained relatively weak into the early 1990s (Simmonds and Jones 1998, Meehl *et al*. 1998).

We here use our most recent station data to diagnose the SAO separately over the three or four decades to the end of 1999. Table 1 shows when diagnosed over the entire 1990s the SAO exhibited amplitudes close those of the 1970s (indeed slightly larger at Davis). Similarly, the percentage variance of the mean annual cycle explained by the SAO was large in the 1990s, and represents a significant recovery from the small values during the 1980s.

Decade	**Amplitude (hPa)**	**% variance**
	Casey	
1960-69	3.4	55.1
1970-79	3.7	63.1
1980-89	2.9	38.6
1990-99	3.5	62.6
	Davis	
1970-79	2.5	48.4
1980-89	2.0	24.1
1990-99	2.7	46.9
	Mawson	
1960-69	2.2	29.4
1970-79	2.1	32.6
1980-89	1.5	15.9
1990-99	2.1	31.4

Table 2: Decadal variations in the amplitude of the surface pressure amplitude of the SAO, and the percentage variance explained of the mean decadal annual cycle by the SAO at the three coastal Australian Antarctic stations.

References

Meehl, G. A., J. W. Hurrell and H. van Loon, 1998: A modulation of the mechanism of the semiannual oscillation in the Southern Hemisphere. *Tellus*, **50A,** 442-450.

Russell-Head, D., and I. Simmonds, 1993: Temporal structure of surface weather parameters at Casey, Davis, Mawson and Macquarie Island. Publication No. 35, Meteorology Section, School of Earth Sciences, University of Melbourne, 181 pp.

Simmonds, I., 2003: Modes of atmospheric variability over the Southern Ocean. *J. Geophys. Res.,* **108,** 8078, doi: 10.1029/2000JC000542.

Simmonds, I., and D. A. Jones, 1998: The mean structure and temporal variability of the semiannual oscillation in the southern extratropics. *Int. J. Climatol.,* **18,** 473-504.

Thompson, D. W. J., J. M. Wallace and G. C. Hegerl, 2000: Annular modes in the extratropical circulation. Part II: Trends. *J. Climate,* **13,** 1018-1036.

Study of Statistical Structure of Surface Wind Speed Vector in Western Antarctica

Ivanov N.E.,[1] *Lagun V.E.* [2]

[1] Saint-Petersbug Branch of State Oceanographic Institute, 23 Line, V.O. 2a, St.-Petersburg, Russia
[2] Arctic and Antarctic Research Institute, Bering str. 38, St. Petersburg, 199397, Russia, lagun@aari.nw.ru

The unique synoptic conditions of West Antarctic station Russkaya (74^o 46' S, 136^o 52' W) characterized frequent hurricane surface wind. Here the regional vector statistical structure of the wind speed is described.

The wind speed mathematical expectation $\vec{\mathbf{V}}(t)$ with cartesian projections {Vx,Vy(t)} is the vector $\vec{\mathbf{V}}(t)$ $\vec{\mathbf{m}}_{\vec{V}} = M\{V_x\vec{\mathbf{e}}_x + V_y\vec{\mathbf{e}}_y\}$, where $\vec{\mathbf{e}}_x$, $\vec{\mathbf{e}}_y$ are unit orts of ÎX and OY axes. Wind speed dispersion $\mathbf{D}_{\vec{V}}$ is symmetric second range tensor $\mathbf{D}_{\vec{V}} = \begin{pmatrix} D_{Vx} & K_{VxVy} \\ K_{VyVx} & D_{Vy} \end{pmatrix} = \begin{pmatrix} \lambda_1 & 0 \\ 0 & \lambda_2 \end{pmatrix}$, where $D_{Vx,y}$, K_{VxVy} is dispersion and co-variations of projections, $\lambda_{1,2}$ are eigenvalues. Geometric image of $\mathbf{D}_{\vec{V}}$ is ellipse with semi-axes $\lambda_{1,2}$, oriented in direction of maximal variability α in initial coordinate system [2]. Numbers $\lambda_{1,2}$ are invariants relative to rotation of coordinate system. Linear invariant $I_1=\lambda_1+\lambda_2$ characterizes the module of total speed variability, it is independent on changes of module $|\vec{\mathbf{V}}|$ or direction φ. Invariant $\chi=\lambda_2/\lambda_1$ characterizes ellipse $\mathbf{D}_{\vec{V}}$. Spectral density $\mathbf{S}_{\vec{V}}(\omega)$ is asymmetric second range tensor $\mathbf{S}_{\vec{V}}(\omega) = \begin{pmatrix} \lambda(\omega) & 0 \\ 0 & \lambda_2(\omega) \end{pmatrix} + 0.5D\begin{pmatrix} 0 & 1 \\ -1 & 0 \end{pmatrix}$. Rotation indicator of different sign $D(\omega)$ shows the prevailing rotation direction: right for $D(\omega)>0$ or left for $D(\omega)<0$. Indicator of the absence of rotation is $\lambda_2(\omega)=0$. The general peculiarities or Russkaya station wind regime are presented as probability distribution in wind rose (Fig.1), spectrum (Fig. 2) and estimates of $\vec{m}_{\vec{V}}$ and $\mathbf{D}_{\vec{V}}$ values (Tables 1, 2). Wind speed time-series trend $\vec{\mathbf{a}}$ is determined as [1] $\vec{\mathbf{V}}(t) = \vec{\mathbf{m}}_{\vec{V}} + \vec{\mathbf{a}}t + \vec{\tilde{\mathbf{a}}}(t)$, where $\vec{\mathbf{a}}$ $\{a_x,a_y\}$ is the vector with cartesian components a_x, a_y, the last are declines of trend projections $V_{x,y}(t) = m_{Vx,y} + a_{x,y}t + \varepsilon_{x,y}(t)$. Trend parameters are module and direction of vector $\vec{\mathbf{a}}$ and they are invariants of anomalies tensor $\mathbf{D}_{\vec{\varepsilon}}$ relative to trend. Regular annual rythmic is presented as hodograph $\vec{\mathbf{m}}_{\vec{V}}(t) - \vec{\mathbf{m}}_{\mathbf{o}}$ and ellipses of annual $\vec{\mathbf{m}}_{\mathbf{1}}(t)$ and semiannual $\vec{\mathbf{m}}_{\mathbf{2}}(t)$ harmonics (Fig. 6), which are commensurable, oblĩng and of left rotation. Thus, spectral pikes on annual and semi-annual frequency are determined. Parameterization ranging from interannual (including vector process trend) to daily variations with account of low-frequency modulation provides uniform presentation for all scales of variability characteristics in climate regime Handbooks. Russkaya station data analysis demonstrates (Fig. 3-5), that the main input in dispersion is formed by annual rhythmic and synoptic scale processes, while their low-frequency modulation increases multiply from intensity of the additive component (the mean annual values time series).

Table 1. Mean wind speed $\vec{\mathbf{m}}_{\vec{V}}$ and estimates of wind speed dispersion tensor $\mathbf{D}_{\vec{V}}$ invariants and wind dispersion module D_V for different averaging time scales of initial data.

Averaging scale			6-hourly	Daily	Monthly	Annual
$\vec{\mathbf{m}}_{\vec{V}}$	m	m/s	10.1			
	D	degrees	86			
D_V		m^2/s^2	111.1	93.3	13.1	1.3
$\mathbf{D}_{\vec{V}}$	I_1	m^2/s^2	176.9	138.1	18.9	4.5
	γ	-	0.15	0.12	0.35	0.51
	α	degrees	79	79	75	175

References
1. Bokov, V.N. et all. 2001. Space-time variability of wind field in Norherm Hemisphere extra-tropical latitudes. Atmosphere and ocean physics, 2001, 37, p. 170-181.
2. Rozhkov, V.A.1997. Probabilities theory of stochastic events, values and functions with hydrometeorologicla examples. SPb., Progress-Pogoda, 1997, 559 pp. (in Russian).

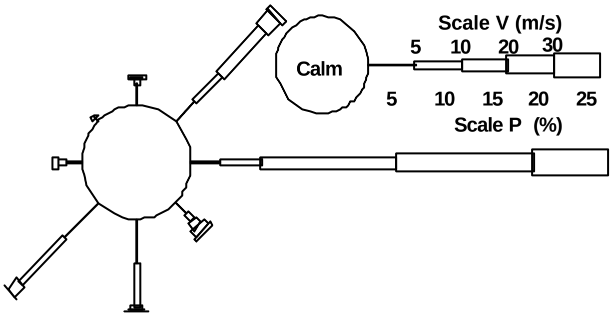

Fig.1 Wind speed rose at Russkaya station

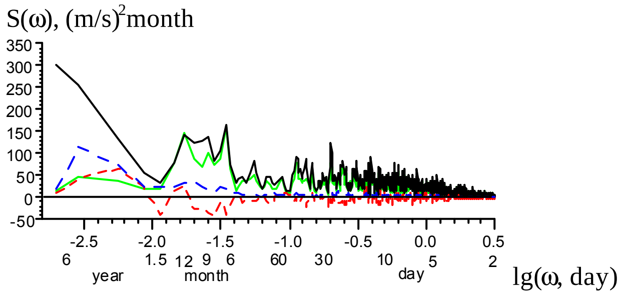

Fig.2 Wind speed Spectrum

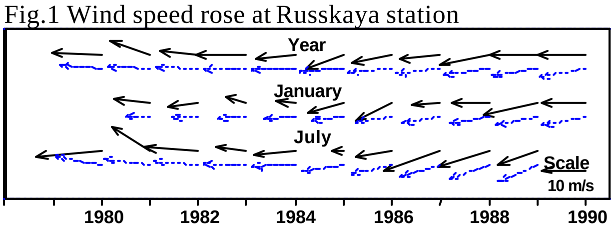

Fig. 3 Time series of mean wind speed (solid) and their linear trend (dashed)

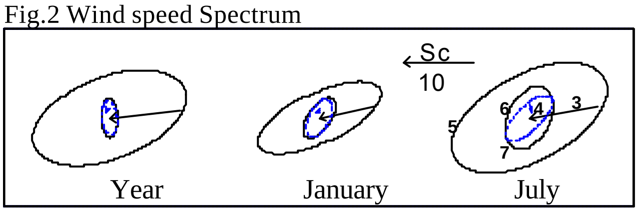

Fig. 4 Mean wind speed, trend coefficients and mean square deviation ellipse of $\mathbf{D}_{\vec{V}}^{0.5}$ (curves 5, 6).

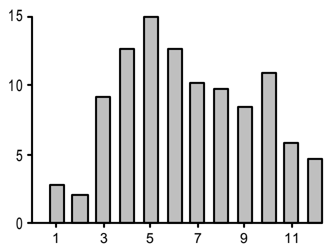

Fig. 5 Annual variation of storm frequency (%)

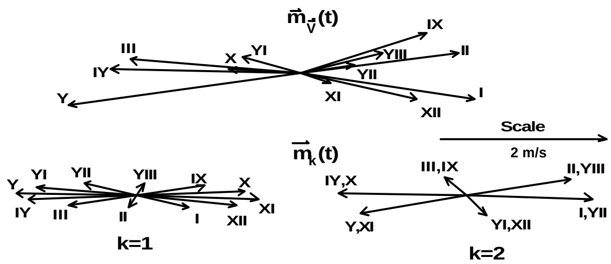

Fig.6 Godograph of $\vec{m}_{\vec{V}}$, annual (k=1) and semiannual (k=2) harmonics

Table 2. Annual variation of mean wind speed $\vec{\mathbf{m}}_{\vec{V}}$, estimates of tensor dispersion $\mathbf{D}_{\vec{V}}$ invariants of monthly mean wind speed, linear tend parameters and maximum wind values (from 6-hourly data).

Month	$\vec{\mathbf{m}}_{\vec{V}}$		$\mathbf{D}_{\vec{V}}$			$\vec{\mathbf{a}}$		$\mathbf{D}_{\vec{a}}$			max($\vec{\mathbf{V}}$)	
	m	D	I_1	φ	χ	|a|	d_a	$I_1^{(\varepsilon)}/I_1^{(v)}$	φ	χ	**V**	φ
	m/s	degrees	$(m/s)^2$	degrees	-	m/s	degrees	%	degrees	-	m/s	degrees
I	8.0	83	8.8	59	0.22	0.45	63	70	55	0.33	39	90
II	8.2	86	6.0	63	0.22	0.23	48	90	66	024	38	80
III	11.9	87	25.3	93	0.32	0.99	276	71	88	0.51	60	90
IY	12.6	86	35.4	76	0.17	0.65	38	86	82	0.11	60	90
Y	13.4	84	25.6	43	0.25	0.51	6	88	49	0.20	55	90
YI	10.5	87	17.3	37	0.61	0.66	2	69	69	0.36	52	90
YII	9.8	85	20.1	57	0.44	0.62	343	76	63	0.20	49	80
YIII	9.5	87	23.6	73	0.20	0.38	8	92	75	0.12	52	90
IX	8.2	88	9.5	24	0.42	0.37	33	83	18	0.48	54	110
X	11.1	85	15.7	89	0.81	0.20	323	97	82	0.78	53	85
XI	8.9	85	15.9	87	0.25	0.39	64	88	93	0.21	47	90
XII	8.3	81	8.1	75	0.25	0.33	73	84	76	0.32	49	90

QUALITY OF QUIKSCAT GRIDDED WINDS OVER THE BAY OF BENGAL

Georgy V. Mostovoy, Patrick J. Fitzpatrick and Yongzuo Li
GeoResources Institute, MSU, Stennis Space Center, Mississippi
E-mail: mostovoi@gri.msstate.edu

Three QuikSCAT gridded datasets from May to August 2001 for 00 UTC and 12 UTC are compared over the Bay of Bengal (BB). This period is characterized by strong and highly persistent southwest surface winds, with occasional 6-10 day spans of low winds known as breaks in the monsoon. The first dataset is based on swath QuikSCAT wind estimates produced by Remote Sensing Systems (RSS) (*QuikSCAT*, 2001). These surface wind components are spatially interpolated to a 1°x1° latitude-longitude grid. Interpolation weights are inversely proportional to the distance between observation cell and grid point. An influence radius of 0.5° is chosen. Only data within ±45-min of 00 UTC or 12 UTC are used. This will be the reference dataset because observed winds are only modified by spatial interpolation within the satellite swath, with no temporal or gap filling.

The second wind dataset is a gridded field converted from objectively derived surface pseudostresses, which are produced online by the Center for Ocean-Atmospheric Prediction Studies at the Florida State University (FSU). The spatial-temporal interpolation is based on the minimization of a cost function with a background wind field representing an 8-day temporal average (*Pegion et al*., 2000). This is a relatively complex and time-consuming procedure. Spatial resolution of this archive is 1°x1° and fields are available every 6 h. We will call this the "FSU" dataset.

A simpler algorithm for QuikSCAT wind gridding is used by Liu, Tang, and Polito (1998) at NASA's Jet Propulsion Laboratory (JPL). Components of the QuikSCAT wind are objectively interpolated both in time and space to a 0.5°x0.5° regular grid using the method of successive corrections. This global surface winds archive has 12-h resolution and is also available online. We will call this the "JPL" dataset.

Scatterplots for northeast Sri Lanka exhibit noticeable diurnal variability in RSS wind speed (Figure 1a). The wind speed at 12 UTC (6 P.M. local time) is consistently lower than the speed at 00 UTC (6 A.M. local time) having the correlation coefficient (R_{12}) of 0.293. RSS wind sets lagged by 24 h have a higher R_{24} of = 0.784. This variability between 00 UTC and 12 UTC winds is not manifested over the central BB. Strong correlations exists both for 12-h (R_{12} = 0.803) and 24-h (R_{24} = 0.861) lags, as shown in Figure 1b.

The smoothing effect of temporal interpolation for JPL winds is evident in Figure 1c and 1d (as an apparent reduction of points scatter) for all regions. JPL winds show in general lower variance and higher correlation for 12-h time lags. A major change of R_{12} from 0.293 (RSS winds) to 0.542 (JPL winds) is observed over northeast Sri Lanka. Spatial distributions of R_{12} and R_{24} also show this difference off Sri Lanka (Figure 2), as well as generally higher correlations for JPL data compared to RSS data. FSU fields also exhibit similar smoothing features (not shown). We can conclude therefore that the spatial-temporal interpolation procedures used to create gridded QuikSCAT winds in the BB alter the original properties of QuikSCAT winds.

To further quantify the impact of diurnal variability on the quality of gridded fields, suppose that temporal interpolation procedures do not take into account the weak relationship between current and 12-h old winds in northeast Sri Lanka, and therefore the weight function is monotonically decaying with time. JPL and FSU winds interpolated with such weights would be generally underestimated at 00 UTC and overestimated at 12 UTC compared with the RSS reference values. Wind speed differences (RSS-JPL) and (RSS-FSU) are used here as a measure of this bias. The difference should be mostly positive at 00 UTC and mostly negative at 12 UTC if the above assumptions about the weight function are valid.

Indeed, histograms of these differences for northeast Sri Lanka (Figure 3a and 3c) show a tendency for positive values prevailing at 00 UTC and for negative values at 12 UTC. Note that this systematic shift between 00 UTC and 12 UTC in the distribution is not observed over the central BB (Figure 3b and 3d). This tendency is also manifested in JPL and FSU long-term mean fields for Northeast Sri Lanka, which show negative bias at 12 UTC and positive bias at 00 UTC (Figures not shown). The magnitude of this bias exceeds 2 ms $^{-1}$ at 00 UTC and 12 UTC.

Acknowledgements. Encouragement by Dr. Roger King and the financial support from the GeoResources Institute is highly appreciated. Authors acknowledge consultations provided by Deborah Smith, Remote Sensing Systems (Santa Rosa, CA) on reading and understanding the QuikSCAT datasets. The JPL winds are obtained from the NASA/NOAA courtesy of W. Timothy Liu and Wenqing Tang. Authors highly appreciate the efforts of Mark A. Bourassa, Center for Ocean-Atmospheric Prediction Studies, FSU for maintaining the COAPS scatterometer web page.

References

Liu W.T., W. Tang, and P.S. Polito, NASA scatterometer provides global ocean-surface wind fields with more structures than numerical weather prediction, *Geophys. Res. Lett., 25,* 761-764, 1998.

Pegion, P.J., M.A. Bourassa, D.M. Legler, and J.J. O'Brien, Objectively derived daily "winds" from satellite scatterometer data, *Mon. Wea. Rev.*, *128*, 3150-3168, 2000.

QuikSCAT, 2001: Remote Sensing Systems' Database for Satellite Microwave Data. (Available online at ftp://ftp.ssmi.com/QSCAT).

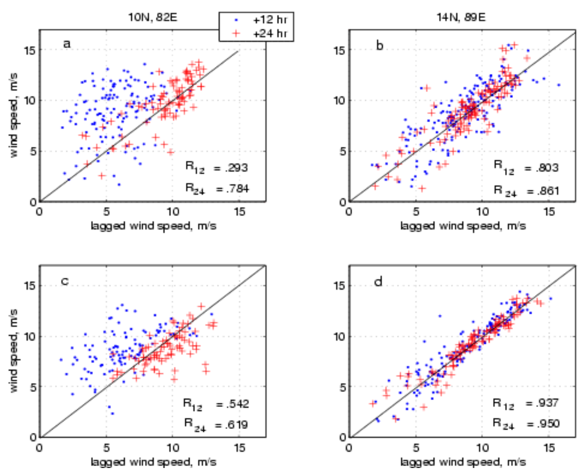

Figure 1. Scatterplots of the QuikSCAT wind speed for 12-h and 24-h time lag for Sri Lanka (a, c) and the central BB (b, d). R_{12} and R_{24} are correlation coefficients of the wind speed for 12-h and 24-h lags. The top (a,b) figures are for raw QuikSCAT data (RSS), and the bottom figures (c, d) are for gridded JPL data.

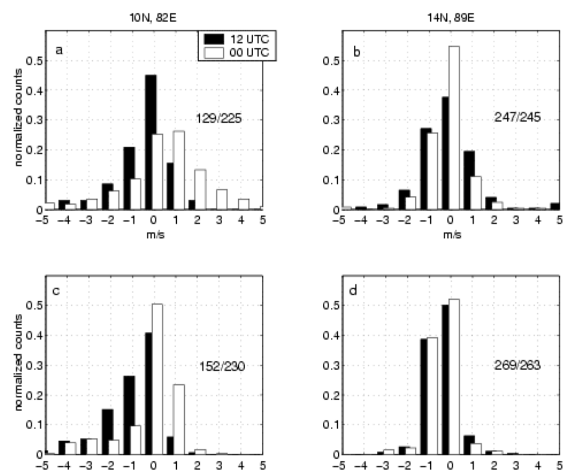

Figure 3. Histograms of wind speed difference between RSS and JPL datasets (a, b), and between RSS and FSU datasets (c, d). Counts in each bin are normalized by total number of observations, shown by numerator for 12 UTC and by denominator for 00 UTC.

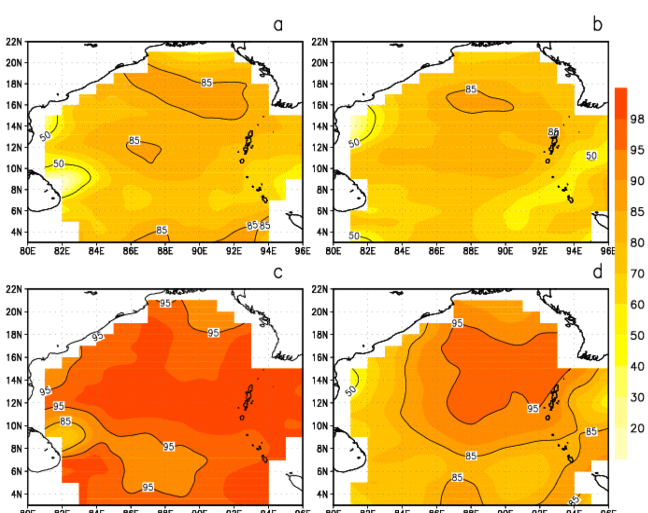

Figure 2. Geographical distribution of autocorrelation coefficients for the QuikSCAT wind speed at 12-h (a, c) and 24-h (b, d) time lags for RSS (a, b) and JPL (c, d) datasets. Correlation coefficients are multiplied by 100. Values of R_{12} and R_{24} are elevated for the JPL dataset compared with RRD winds. Note that low R_{12} values (< 0.5) for RSS winds (a) is concentrated in northeast Sri Lanka. This implies that wind speed interpolation from 00 UTC and 12 UTC and vice versa is not statistically justified in regions subject to diurnal wind variations such as Sri Lanka.

COMPARISON OF QUIKSCAT GRIDDED WINDS OVER THE GULF OF MEXICO

Georgy V. Mostovoy and Patrick J. Fitzpatrick
GeoResources Institute, MSU, Stennis Space Center, Mississippi
E-mail: mostovoi@gri.msstate.edu

A comparison between different QuikSCAT gridded datasets similar to the study of Mostovoy et al. (2004) has been performed over the Gulf of Mexico. The same datasets (RSS, FSU and JPL) of QuikSCAT winds are used to demonstrate that results of comparison obtained over the Bay of Bengal (Mostovoy et al., 2004) are also observed in other oceanic regions. An analysis covers a span from May to August for the 3-year time period (from 2001 to 2003). Additionally the FSU, JPL and RSS datasets are compared against in situ wind speed measurements from U.S. National Data Buoy Center ocean buoys. Quality controlled observations from 11 moored buoys (3-m and 10-m discus) are used for comparison. They are located over the northern part of the Gulf of Mexico. The QuikSCAT data provide an estimate of the 10-m neutral equivalent wind (Verschell et al., 1999). Therefore wind speed observations from 5-m height (3-m discus buoys) have been adjusted to the 10-m height, using power-law profile with an exponent equal to 0.1, but the buoy wind speed have not been corrected for the effects of atmospheric stability. It has been shown that stability correction has a little impact on the results of comparison.

The scatterplot technique is used to reveal smoothing effects of the temporal interpolation on the gridded winds. For the comparison with buoy observations, data from grid point nearest to the buoy location are selected. As an example Figure 1 is for the buoy 42020. It shows a correlation between 00 UTC and 12 UTC wind speed for observations, RSS, FSU and JPL datasets. Relative to the observations (Figure 1a) QuikSCAT gridded winds (Figures 1b, 1c, and 1d) except for RSS dataset exhibit less scatter between 00 UTC and 12 UTC values.

The smoothing effect of temporal interpolation apparent as a reduction of the scatter in FSU and JPL datasets is quite clear (see Figures 1c and 1d) in comparison with observations and RSS winds (Figures 1a and 1b). A similar tendency for the excessive smoothing is also evident for other buoys. The Figure 2 is for the buoy 42001. Correlation coefficients between 00 UTC and 12 UTC winds have been calculated to quantify this reduction in the data points scatter. They are plotted in Figure 3 along with 95% confidence limits for all the buoys used in this study. Correlations coefficients for FSU and JPL datasets are significantly higher than that for observations and RSS winds.

Another way to describe the smoothing effect of temporal interpolation is shown in Figure 4 where histograms of QuikSCAT (RSS, FSU and JPL) minus buoy wind speed difference are plotted for 42020 buoy. Both FSU and JPL winds are in the mean biased relatively low compared to the RSS data for buoy wind speeds exceeding 4 m/s (Figures 4a and 4c). In contrast, high bias in QuikSCAT winds is typical for low speeds (Figures 4b and 4d). The example in Figure 5 for 42001 buoy is similar to Figure 4.

This study has shown that FSU and JPL gridded datasets reproduce crudely diurnal variability of winds providing a reduced difference between OO UTC and 12 UTC values in comparison with observations and RSS data. Rather, the FSU and JPL gridded products describe daily mean fields.

Acknowledgements. Encouragement by Dr. Roger King and the financial support from the GeoResources Institute is highly appreciated. Authors acknowledge consultations provided by Deborah Smith, Remote Sensing Systems (Santa Rosa, CA) on reading and understanding the QuikSCAT datasets. The JPL winds are obtained from the NASA/NOAA courtesy of W. Timothy Liu and Wenqing Tang. Authors highly appreciate the efforts of Mark A. Bourassa, Center for Ocean-Atmospheric Prediction Studies, FSU for maintaining the COAPS scatterometer web page.

References

Mostovoy G.V., P.J. Fitzpatrick, and Y. Li, Quality of QuikSCAT gridded winds over the Bay of Bengal, Research Activities in Atmospheric and Oceanic Modelling, 2004 (current report).

Verschell , M.A., Bourassa M.A., Weisman D.E., and O'Brien, J.J., Model validation of the NASA Scatterometer winds, *Journal of Geophys. Res., 104*, 11359-11374, 1999.

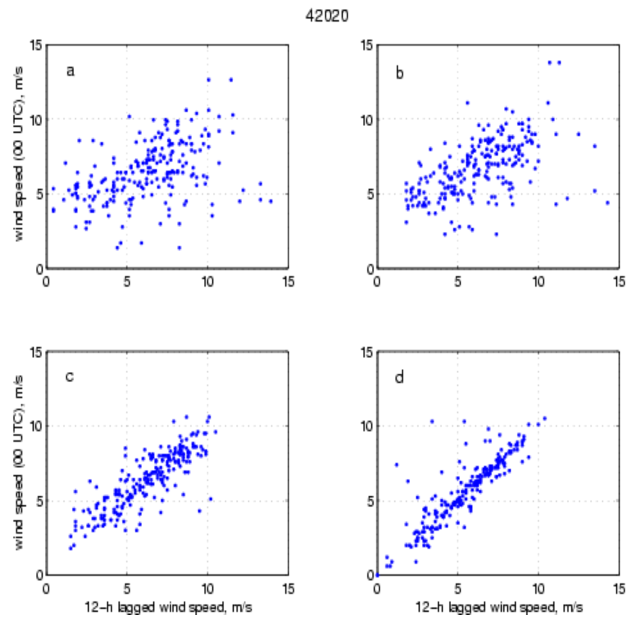

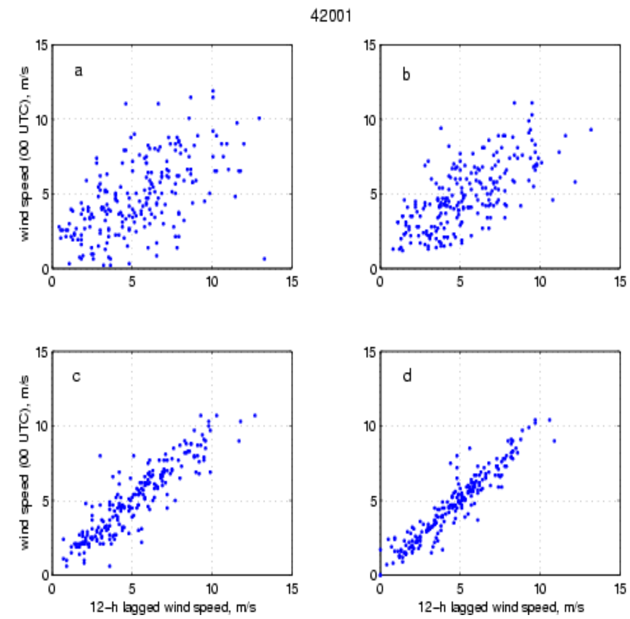

Figure 1. Scatterplots of the QuikSCAT wind speed for ±12-h time lags for 42020 buoy. The top frames are for buoy observations (a), and for RSS winds (b). The bottom frames are for FSU (c) and JPL (d) gridded winds. Note a substantial reduction of variance in FSU and JPL data as compare with observations and RSS values.

Figure 2. The same as in figure 1, but for 42001.buoy.

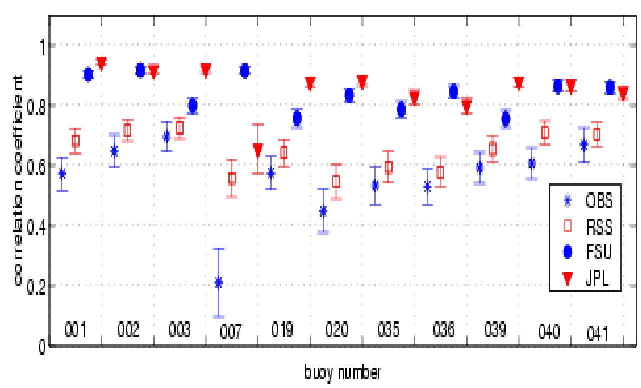

Figure 3. Correlation coefficients between 00 UTC and 12 UTC winds for different datasets. Abscissa corresponds to the buoy number (region prefix 42 is omitted). Error bars stand for 95% confidence limits.

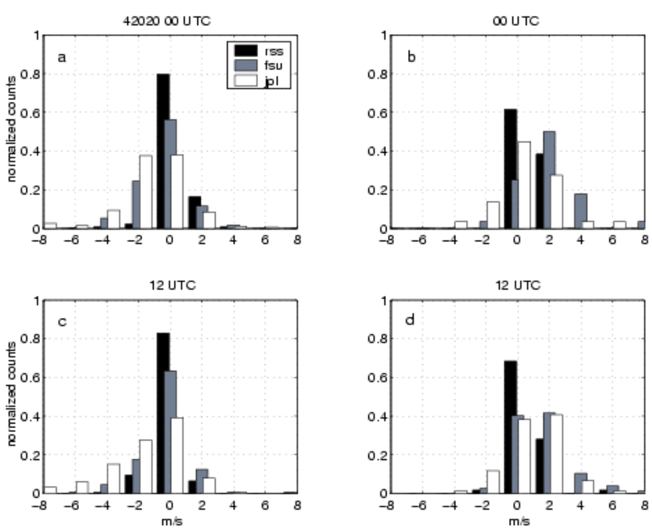

Figure 4. Histograms of QuikSCAT-buoy wind speed difference for 42020 buoy at 00 UTC (a,b) and 12 UTC (c,d). Plots (a,c) are for buoy wind speed > 4 m/s, and plots (b,d) are for wind speed ≤ 4 m/s.

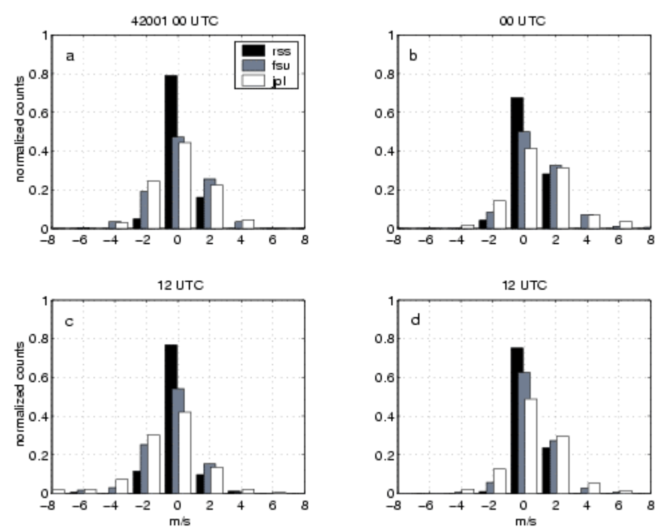

Figure 5. The same as in figure 4, but for 42001 buoy.

Southeast Pacific sea ice and ENSO co-variabilities

Anthony Rafter[1], Ian Simmonds[1] and Andrew B. Watkins[2]

[1] School of Earth Sciences
The University of Melbourne
Victoria, Australia, 3010
Email: simmonds@unimelb.edu.au

[2] National Climate Centre
Bureau of Meteorology
GPO Box 1289K Melbourne
Victoria, Australia, 3001

The subantarctic region in the southeast Pacific Ocean is host to very high levels of atmospheric variability (e.g., Simmonds and Murray, 1999). A number of studies have explored the relationship between interannual variations in sea ice conditions in this region and measures of ENSO activity (e.g., Simmonds and Jacka 1995 (SJ), Yuan and Martinson 2000). SJ found that for the period 1973-1992 the Southern Oscillation Index (SOI) was significantly and positively correlated with late winter and spring sea ice extent in the sector 225 - 255^{o}E when the former led by up to 12 months (their Fig. 3c). We here update their analysis using more the more recent sea ice data in this sector obtained from the passive microwave sensors aboard the SMMR and SSM/I satellites, covering the period 1979-2000.

In the manner of SJ we present in the top panel of Fig. 1 the plot of the correlations (over 1979-2000) of the SOI and sea ice variabilities. These correlations with winter and spring sea ice exceed 0.4 when the SOI leads by up to eight months (and even longer in winter). (The synchronous correlations are quite modest.) The plot shows considerable similarity to that of SJ.

Cullather *et al*. (1996) showed that the association between the SOI and an aspect of the subantarctic circulation (between 180 and 240^{o}E) changed dramatically around 1990. We have performed correlation analyses similar to the above for the two 11-year periods which make up our total record (i.e., 1979-1989 and 1990-2000). The results are shown in the middle and bottom panels of Fig. 1. There are a number of common features in the plots, including the observation that late-year sea ice extent variations are positively correlated with mid year SOI. However, overall, the apparent associations between sea ice and the SOI are different in the two periods. In general the winter and spring sea ice variability shows only very modest associations with the SOI in the previous 12 months in the 1979-1989 interval. By contrast, the correlations are for the most part larger in the second half of the record, and winter sea ice extent is correlated with the SOI (coefficients exceeding 0.6) for leads of up to 12 months.

Cullather, R. I., D. H. Bromwich and M. L. VanWoert, 1996: Interannual variations in Antarctic precipitation related to El Niño Southern Oscillation. *J. Geophys. Res.,* **101,** 19109-19118.

Simmonds, I., and T. H. Jacka, 1995: Relationships between the interannual variability of Antarctic sea ice and the Southern Oscillation. *J. Climate,* **8,** 637-647.

Simmonds, I., and R. J. Murray, 1999: Southern extratropical cyclone behavior in ECMWF analyses during the FROST Special Observing Periods. *Wea. Forecasting,* **14,** 878-891.

Yuan, X. J., and D. G. Martinson, 2000: Antarctic sea ice extent variability and its global connectivity. *J. Climate,* **13,** 1697-1717.

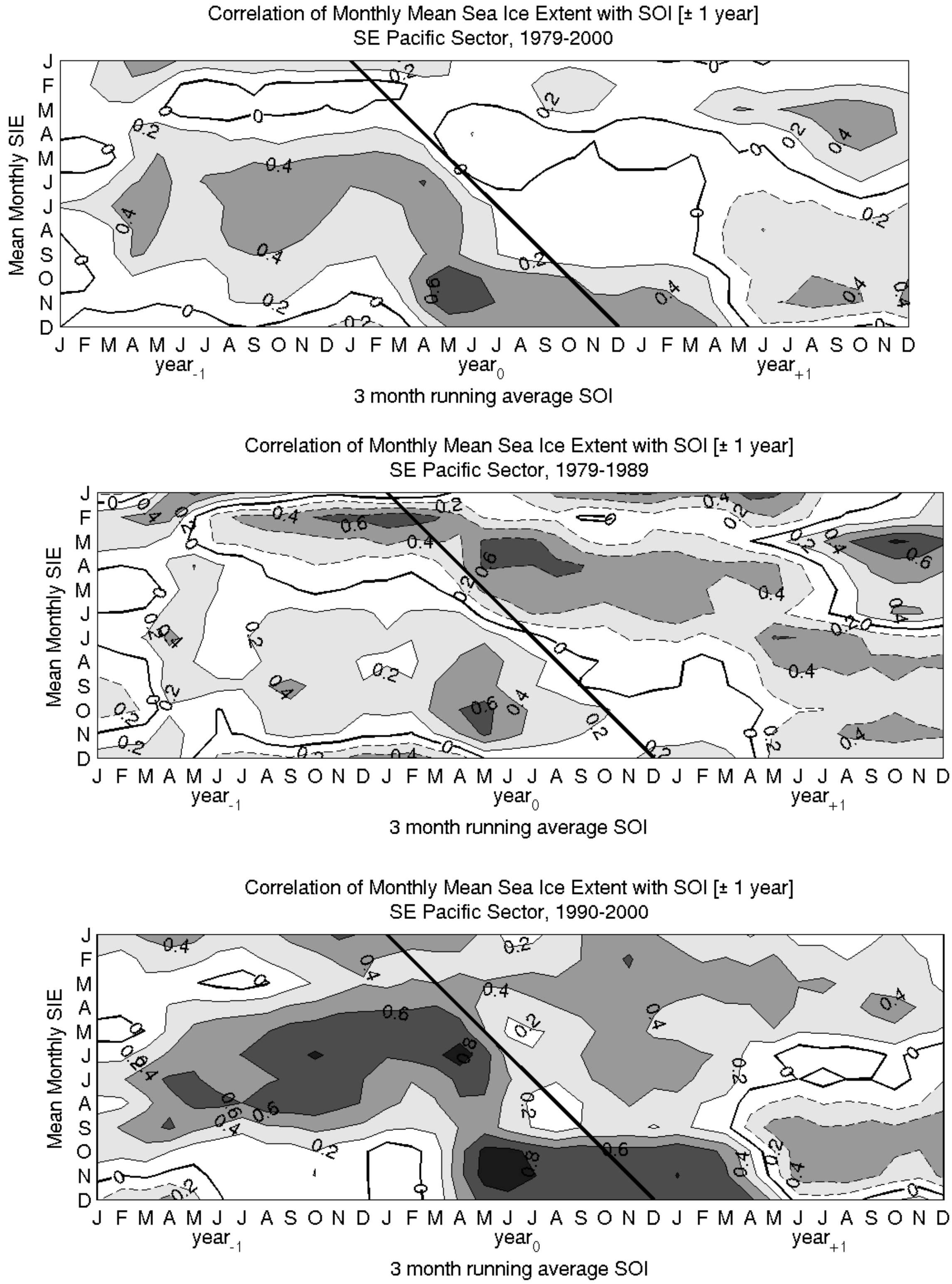

Figure 1: (top) Correlation (1979-2000) between the 3-month running average of the SOI and the Antarctic sea ice extent, averaged over the southeast Pacific Ocean (225 - 255^{o}E). The calendar months for the SOI are given on the abscissa, extending from the year before the sea ice data (SOI leads), the same year, to the year after (SOI lags). The contour interval is 0.2 and the bold diagonal line joins up points of synchronous correlation. (middle) As for ‘top’ but for 1979-1989. (bottom) As for ‘top’ but for 1990-2000.

A New European Precipitation Dataset for NWP Model Verification and Data Assimilation Studies

Franz Rubel

Working Group Biometeorology, Veterinärmedizinische Universität Wien (VUW)
Veterinärplatz 1, A-1210 Vienna, Austria, franz.rubel@vu-wien.ac.at

Within the framework of ELDAS[1] (van den Hurk, 2002) an initiative was launched to collect and analyse daily precipitation measurements. Goal is to analyse precipitation fields on a regular 0.2 degree latitude/longitude grid. These fields serve as ground truth for NWP model verification; NWP centres involved are KNMI, DWD, ECMWF, INM and MeteoFrance, respectively. Further these daily precipitation fields are used to generate 3-hourly fields by disaggregating them with additional information from weather radars. The latter will be used as forcing data for the ELDAS soil moisture assimilation.

Here we present the ELDAS precipitation dataset with daily resolution. It consists of about 1 000 synoptic and 19 000 climate precipitation gauges from 15 countries of the European Union and forthcoming member states (Fig. 1). Thus, this dataset is one of the most extensive collections of European precipitation data. It is available for the ELDAS reference period Oct. 1999 to Dec. 2000 and designed to NWP community specifications, that is maximum spatial coverage and high temporal resolution. The gridded data are stored in GRIB format and made available by the ECMWF MARS archive.

For the analysis the Precipitation Correction and Analysis (PCA) model (Rubel and Hantel, 2001), developed during the Baltic Sea Experiment (Raschke et al., 2001), has been applied. Over France gridded data from MeteoFrance have been blended. The PCA model consists of two components: (1) a module for the reduction of the systematic measurement error of the rain gauges and (2) a geostatistical module for the analysis of areal precipitation estimates (including the interpolation error). The application of PCA fields to verify meso-scale NWP models has been demonstrated by Jacob et al. (2001). A more comprehensive study has been performed over the European Alps to compare the performance of daily precipitation estimates predicted by the ECMWF model (t+6 to t+30) and estimated by satellites from the Global Precipitation Climatology Project (GPCP-1DD). Both precipitation products have been compared to each other using scores from verification against ground truth (Rubel and Rudolf, 2001; Rubel et al., 2002).

References

Jacob, D., and Co-authors, 2001: A comprehensive model intercomparison study investigating the water budget during the BALTEX-PIDCAP period. *Meteorol. Atm. Phys.,* **77,** 19-43.

Raschke, E., and Co-authors, 2001: The Baltic Sea Experiment (BALTEX): A European contribution to the investigation of the energy and water cycle over a large drainage basin. *Bull. Amer. Meteor. Soc.,* **82,** 2389-2413.

Rubel, F., and M. Hantel, 2001: BALTEX 1/6-degree daily precipitation climatology 1996-1998. *Meteorol. Atm. Phys.,* **77,** 155-166.

Rubel, F., and B. Rudolf, 2001: Global daily precipitation estimates proved over the European Alps. *Meteorol. Z.,* **10,** 403-414.

Rubel, F., P. Skomorowski, and B. Rudolf, 2002: Verification scores for the operational GPCP-1DD product over the European Alps. *Meteorol. Z.,* **11,** 367-370.

Van den Hurk, B., 2002: European LDAS established. *GEWEX News,* **12/2,** 9-9. http://www.gewex.org/

[1]Development of a European Land Data Assimilation System to predict floods and droughts, project financed by the European Commission (EVG1-CT-2001-00050), see http://www.knmi.nl/samenw/eldas/

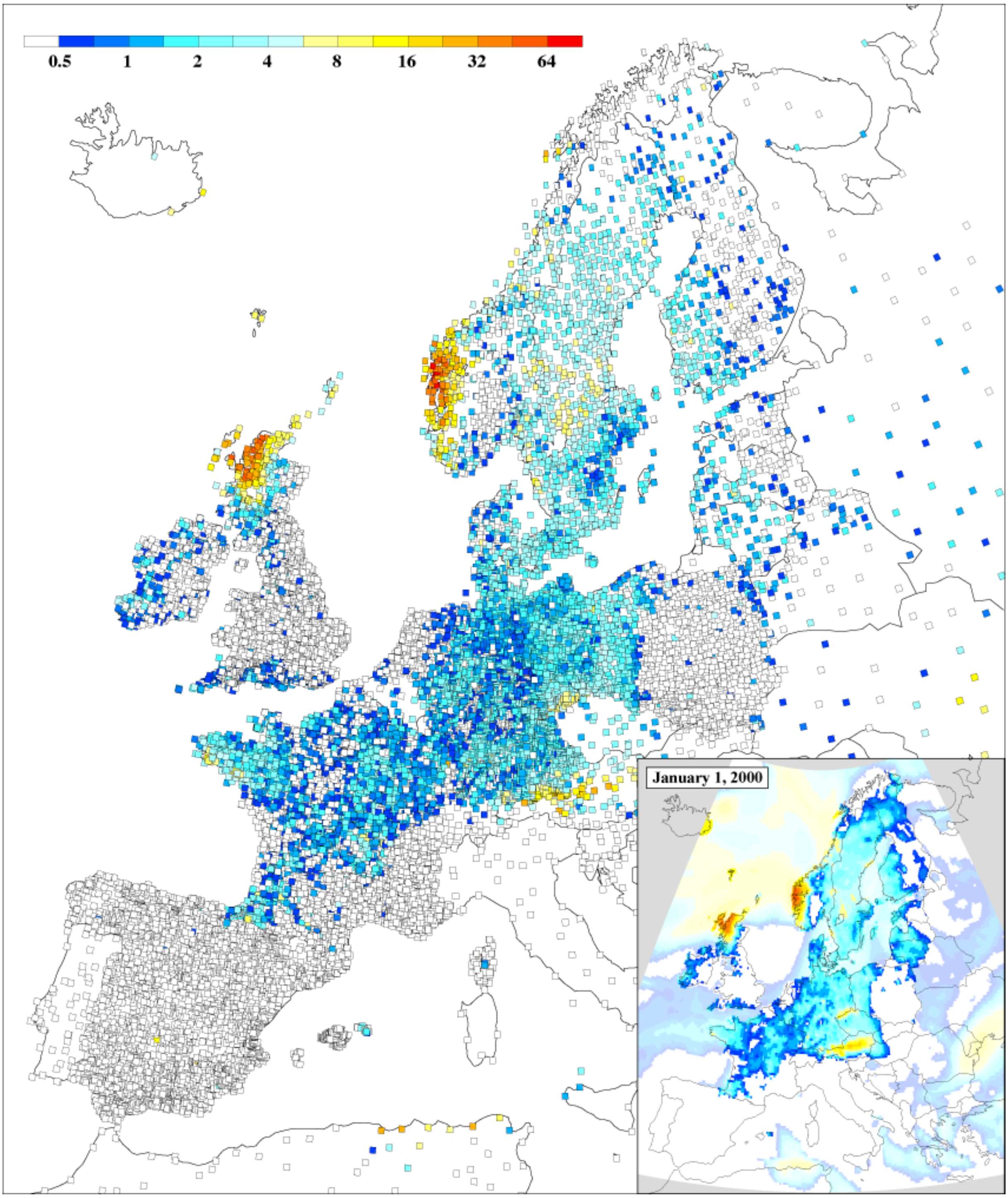

Fig. 1 ELDAS precipitation gauge dataset for January 1, 2000, 6 UTC. Units mm/day. Lower right corner: Appropirate gridded precipitation data analysed from 20 049 bias corrected gauge observations. ECMWF background field in bright colors.

Acknowledgments: C. Graute (BMDC), B. vd Hurk (KNMI), P. Le Moigne and J. Noilhan (Meteo France), A. Menochet (BADC), U. Gjertsen and E. Førland (DNMI), B. Navascues and E. Rodriguez Camino (INM), P. Viterbo (ECMWF), L. Haimberger (IMGW), B. Rudolf and P. Otto (GPCC), T. Sheridan and A. Murphy (Met Eireann), P. Skomorowski (VUW) contributed to the data collection.

Kinetic energy fluxes into the Southern Ocean

Ian Simmonds
School of Earth Sciences
The University of Melbourne
Victoria, Australia, 3010
Email: simmonds@unimelb.edu.au

The northern boundary of the Southern Ocean (SO) may be defined as the Subtropical Front, which lies roughly along 40^{o}S around much of the hemisphere. Defined in this way it occupies about 20% of the surface area of the global ocean. A reflection of the global importance of fluxes into the SO is that water masses formed in there account for more than 50% of the volume of the world ocean (Godfrey and Rintoul 1998). The region is subject to a wide variety of variability mechanisms (Simmonds 2003). We here make use of the NCEP-2 reanalysis data set (Kanamitsu *et al.* 2002) over the period 1979 to 2002, to diagnose aspects of the largescale atmospheric variability and the flux of mechanical energy from the atmosphere to the ocean. The latter is of central importance in determining the nature of oceanic wave climate.

The very baroclinic conditions over the high and mid latitudes in the SO means that it is a region of intense cyclonic activity. This activity is reflected in the structure of the 'directional constancy' of the low-level (10m) wind, which is defined as the ratio of the magnitude of the mean vector wind and the mean wind speed. In NCEP-2 the constancy exhibits a midlatitude band (particularly wide in the Indian Ocean) over which the 'constancy' exceeds 0.6 (Fig. 1), while displaying very low values in the immediate subantarctic region. This overall structure can be understood in terms of the high frequency of cyclones near, and to the south of, 60^{o}S (Simmonds and Keay 2000, Simmonds *et al.* 2003).

The cyclones play an important role in determining the rate at which kinetic energy is deposited into the SO. If the atmospheric density and momentum exchange coefficient are regarded as constant, this rate is proportional to the mean of the cube of the wind speed. This mean is presented in Fig. 2 for the winter season. There is band of high mechanical energy input at about 45^{o}S from the eastern Indian to the west Pacific Ocean which attains its maximum (in excess of 4000 m^3s^{-3}) in the vicinity of Kerguélen. The values attest to the well-deserved reputation of the SO as having some of the strongest winds and largest waves over the global ocean. Significant fluxes are also diagnosed over the sea ice region. More complete details of this work may be found in Simmonds and King (2004).

Godfrey, J. S., and S. R. Rintoul, 1998: The Role of the Oceans in Southern Hemisphere Climate. *Meteorology of the Southern Hemisphere.* D. J. Karoly, and D. G. Vincent, Eds., American Meteorological Society, 283-306.

Kanamitsu, M. et al., 2002: NCEP-DOE AMIP-II Reanalysis (R-2). *Bull. Amer. Meteor. Soc.,* **83,** 1631-1643.

Simmonds, I., 2003: Modes of atmospheric variability over the Southern Ocean. *J. Geophys. Res.,* **108,** 8078, doi: 10.1029/2000JC000542.

Simmonds, I., and K. Keay, 2000: Mean Southern Hemisphere extratropical cyclone behavior in the 40-year NCEP-NCAR reanalysis. *J. Climate,* **13,** 873-885.

Simmonds, I., K. Keay and E.-P. Lim, 2003: Synoptic activity in the seas around Antarctica. *Mon. Wea. Rev.,* **131,** 272-288.

Simmonds, I., and J. C. King, 2004: Global and hemispheric climate variations affecting the Southern Ocean. *Antarctic Science,* (submitted).

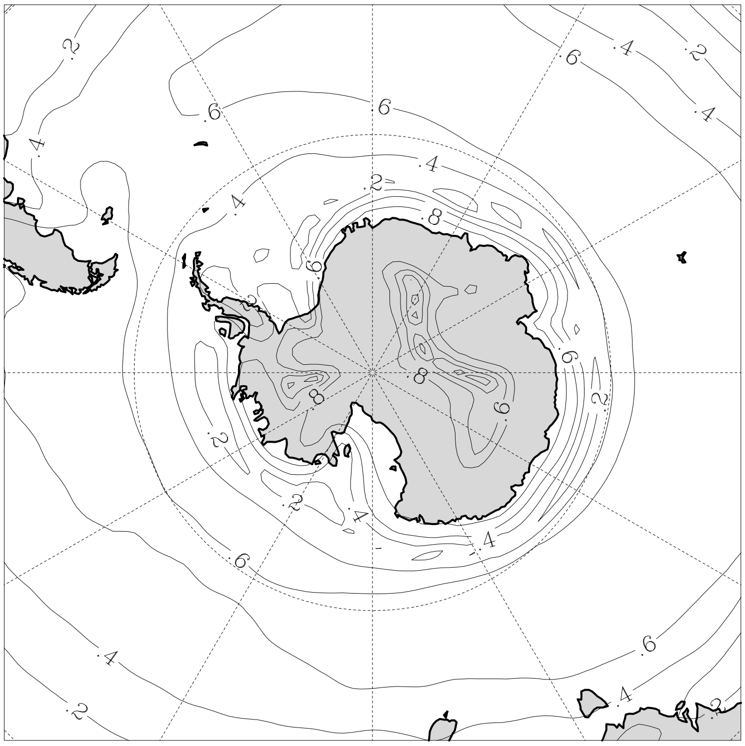

Figure 1: Annual mean directional constancy.

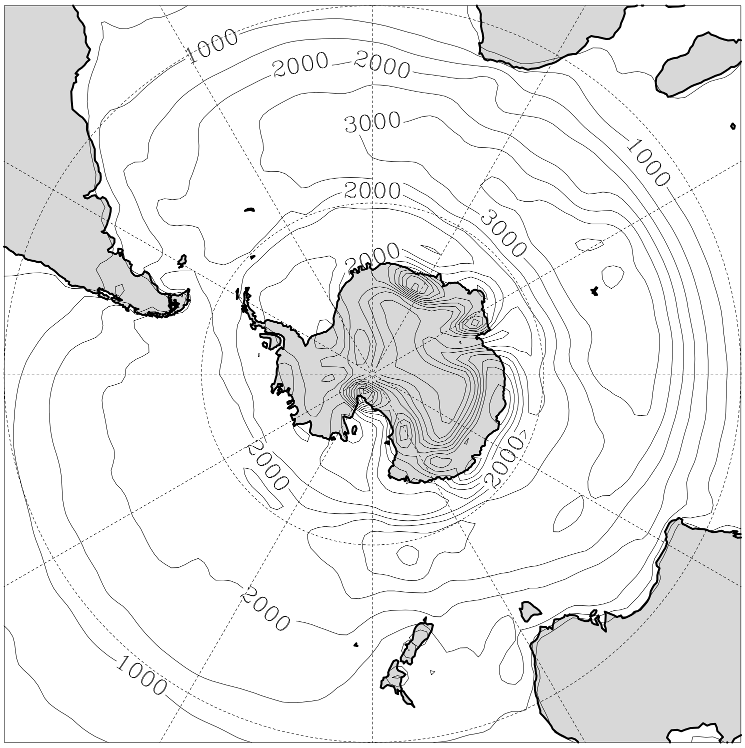

Figure 2: JJA climatology of the mean of the cube of the 10m wind speed. The contour interval is 500 m^3s^{-3}.

A New Technique for Estimation of Sea surface Salinity in the Tropical Indian Ocean from OLR

Bulusu Subrahmanyam, V.S.N. Murty*, and James J. O'Brien
Center for Ocean-Atmospheric Prediction Studies, The Florida State University,
Tallahassee, FL 32306-2840, USA.
*Physical Oceanography Division, National Institute of Oceanography,
Goa 403 004, India
(e-mail: sub@coaps.fsu.edu, vsnmurty@darya.nio.org, obrien@coaps.fsu.edu)

Abstract

Salinity is one of the three state variables (along with temperature and pressure) that determine the density of seawater and is missing from direct measurements of space-borne satellites. It is the key parameter that determines the hydrological cycle over the oceans and hence has the climatic implications. This study provides a new technique to determine the Sea Surface Salinity (SSS) in the tropical Indian Ocean based on the algorithms developed using the satellite measured Outgoing Longwave Radiation (OLR). The algorithms are the statistical relationships between the OLR and an oceanic parameter, the Effective Oceanic Layer (EOL), and between EOL and climatological (World Ocean Atlas 1998) SSS. The SSS product as derived from space-borne satellite measurements of OLR, based on the algorithms developed by Murty et al. [2003], is discussed for the tropical Indian Ocean (TIO) during the period 1979-2000.

Method

This study addresses this new method for deriving the SSS from OLR in the Indian Ocean wherein the convection over the ocean is a regular seasonal phenomenon in association with the summer monsoon and the Intertropical Convergence Zone (ITCZ). Murty et al. [2002] describes this new method with a preliminary assessment of estimation of SSS over the Bay of Bengal using the OLR. The OLR measures the cloud top temperature and represents the measure of convection over the oceans and land areas. The intense convection will have the lowest cloud top temperature and hence the lowest OLR. Therefore, the zones of the lowest OLR could be the regions of intense convection over the tropical Oceans. Conversely, the zones of the highest OLR (say, 220 W/m^2) could be regions of little convection or cloud-free skies. This new technique is explained in Murty et al. [2003] with more details.

Results

The SSS anomalies relative to Levtius climatology during 1995 are shown for the months of January, April, July and October (Figs. 1a-d). The deviations of the estimated SSS from the WOA98 SSS for each month are within ±1.0 psu in a larger area of the tropical Indian Ocean. The deviations are typically large in the Bay of Bengal during July and October where the river run off and intensive convection lead precipitation control the SSS. The largest deviation in the SSS in July and October are the artifact of contouring near the coastal boundary of the Bay of Bengal. The deviations between the estimated and WOA98 SSS are more or less in the same range from one year to the other. We have shown comparison of this new product with WOCE sections and individual cruise hydrographic observations in Murty et al. [2003].

Conclusions

In this study we have shown a better way of obtaining daily SSS information from satellite observations of OLR. The daily SSS product is also useful for studying the impact of tropical cyclones on the upper ocean and study the air-sea coupling during the tropical cyclones [Subrahmanyam et al. 2003]. This study also boosts the coupled models, ENSO forecast models as well as ocean global circulation models (or regional scale circulation models). We envisage that this way of obtaining daily SSS would be very helpful until the space born satellite measurements are available.

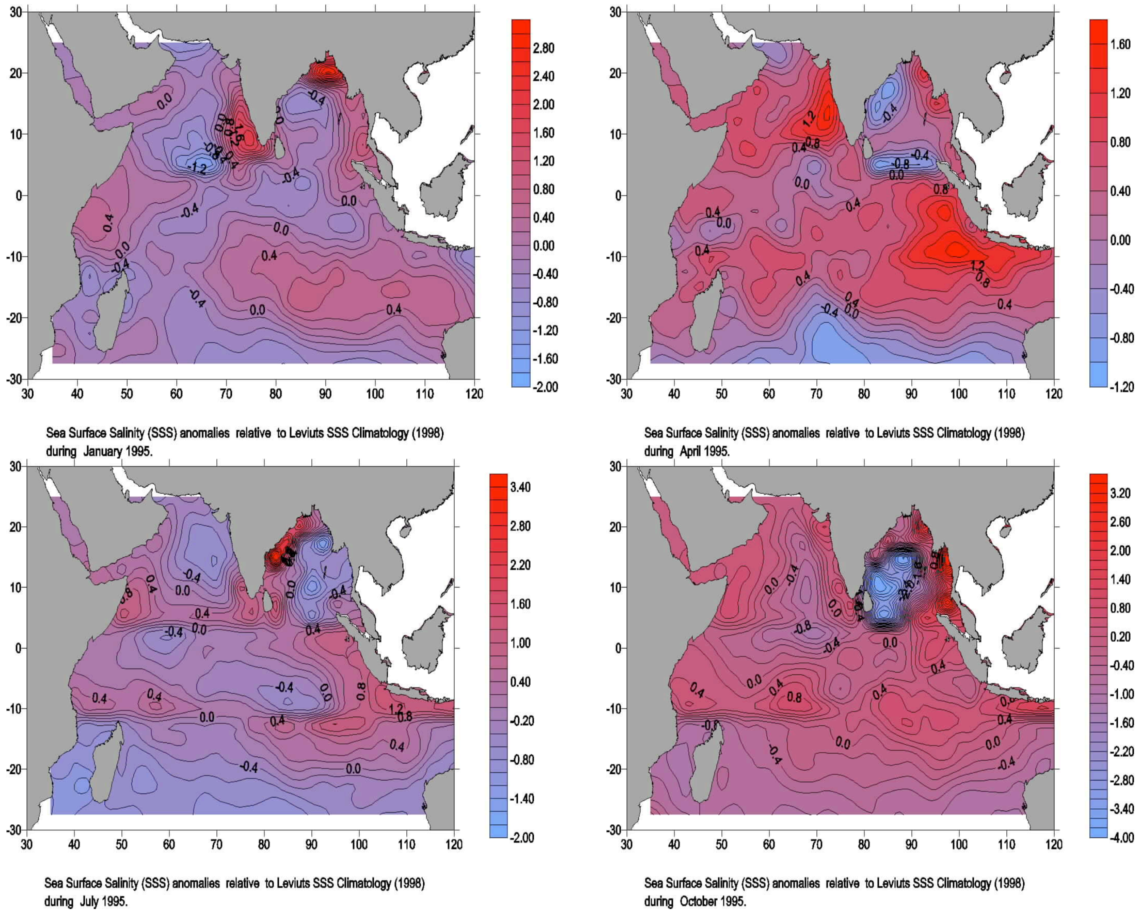

Fig. 4. Difference between estimated SSS and WOA98 SSS climatology in 1995 during a) January, b) April, c) July and d) October.

References

Subrahmanyam, B., V.SN. Murty, R.J. Sharp, J.J. O'Brien [2003]. Air-Sea Coupling during the tropical cyclones in the Indian Ocean- a case study using satellite observations, J. Pure and Applied Geophysics (Submitted) .

V.S.N. Murty, B. Subrahmanyam, V. Tilvi, and J.J. O'Brien [2003]. Sea Surface Salinity estimation from Outgoing Longwave Radiation in the tropical Indian Ocean-its algorithms and variability, J. Geophys. Res. (Submitted).

V.S.N. Murty, B. Subrahmanyam, M.S.S. Sarma, V. Tilvi and V. Ramesh Babu [2002]. Estimation of sea surface salinity in the Bay of Bengal using Outgoing Longwave Radiation", *Geophys. Res. Lett.*, vol. 29, doi:10.1029/2001GL014424, 22-1.

Acknowledgements

The interpolated OLR data is provided by the NOAA-CIRES Climate Diagnostics Center, Boulder, Colorado, USA from their web-site at http://www.cdc.noaa.gov/. BS is supported by the T/P and JASON-1 altimetry project at the NASA JPL under #961434. The COAPS at the FSU receives its base support from the NOAA Office of Global Programs awarded to James J. O'Brien.

Precipitation Correction in the ERA-40 Reanalysis,

Alberto Troccoli and Per Kållberg, ECMWF, Shinfield Park, Reading RG2 9AX, UK.
E-mail: a.troccoli@ecmwf.int

1 Introduction

The ECMWF 40-year reanalysis project ('ERA-40') has recently reached its completion. These reanalyses of the state of the atmosphere from September 1957 to August 2002 provide a very high quality reference atmospheric state for quite a long period and adds a competitor to the hitherto available NCEP/NCAR 50-year and ECMWF ('ERA-15') 15-year reanalyses.

Evaluation of the precipitation over tropical oceans show excessive amounts when compared to independent estimates (GPCP, http://precip.gsfc.nasa.gov and Huffman *et al.*, 1997) during the latter parts of ERA-40. This has been found to be due to a fundamental problem in the variational analysis of humidity over tropical oceans in areas of high density observations, such as satellite radiances. The increased precipitation with time might also be part of the climate signal, but our estimates indicate that the first order effect is indeed due to the humidity analysis deficiency. We will therefore assume that the real average precipitation during the 45 years does not vary significantly.

Precipitation is an essential component of the fields used to force ocean models. Since in the European Project ENACT (Enhanced Ocean Data Assimilation and Climate Prediction) the choice was made to use the ERA-40 fields to force the various ocean models taking part in the project, a solution to the excessive precipitation issue had to be sought. This paper presents the solution adopted in the context of ENACT but which might have wider applications. The procedure, its assumptions and its results are presented in section 2. A brief summary is given in section 3.

2 The precipitation correction

The production phase of the ERA-40 reanalysis consisted of five consecutive periods or streams: 1956-1963, 1964-1972, 1973-1978, 1979-1988 and 1989-2001. Three main assumptions (or constraints) are adopted in order to calculate the magnitude of the precipitation correction, which will be different for each stream: 1) The ERA-40 precipitation field for the reference stream should conform to (be consistent with) the observed precipitation field. A pseudo-climatological precipitation is the product of this evaluation; 2) The water budget, precipitation minus evaporation, has to be zero in a global sense for each stream; 3) The evaporation field is treated as error-free.

In particular, the second assumption may be applied in two ways: a) by calculating the precipitation minus evaporation (PmE) for the entire globe (i.e., land plus ocean) or b) by calculating the same budget but for the ocean area only. In the latter case, the river runoff contribution has to be considered too, i.e., (P+R-E) should balance out. Since the original objective of this investigation was to use precipitation as an ocean model forcing, the second approach was taken. It has been tested, however, that the two approaches, a) and b), are equivalent.

Note that, because the largest differences in precipitation appear only in the oceanic tropical band, the correction is evaluated only for the latitudinal range between 30°S and 30°N over the ocean. No attempt is made to refine the correction to be longitude-dependent.

The minimisation procedure only involves a single coefficient, α:

$$\alpha = \frac{\left(\overline{P} + \overline{R} - \overline{E}\right)}{\left(\overline{P} - \overline{P_O}\right)} \tag{1}$$

where $\overline{P}$ is the mean original ERA-40 precipitation, $\overline{P_O}$ is either the observed or the pseudo-climatological precipitation. Note that P_O coincides with the original ERA-40 precipitation outside the ±30° band. $\overline{E}$ is the mean evaporation and $\overline{R}$ is the mean river runoff ($\overline{R}$ is assumed to be about 10% of $\overline{E}$). The means of these variables are weighted according to the latitudinal length of the grid.

The reference stream was chosen to be that for 1964-1972 because, for this period, there are enough observations to constrain the model fields but, at the same time, not too many humidity observations to disrupt the precipitation field. Next, the pseudo-climatological precipitation is derived by combining the 1964-1972 stream with the 1979-2001 GPCP climatology, by solving (1). As the ERA-40 precipitation field has consistently larger values than GPCP in the tropical band, the value of α is positive and equal to about 0.25 (see last column in table 1).

OCEAN MEAN VALUES (mm day^{-1})							
Stream	$\overline{P}$	$\overline{E}$	$\overline{PmE}$	$\overline{P_C}$	$\overline{P_CmE}$	$(\overline{P_C}+\overline{R}-\overline{E})$	α
1956-1963	3.20	3.33	-0.30	3.16	-0.34	-0.004	0.39
1964-1972	3.24	3.27	-0.20	3.12	-0.32	0.005	0.25
1973-1978	3.40	3.16	0.07	3.10	-0.23	0.09	1.40
1979-1988	3.43	3.29	-0.04	3.14	-0.33	0.003	0.95
1989-2001	3.72	3.27	0.29	3.10	-0.34	-0.008	1.02
GPCP (1979-2001)	2.82						

Table 1: Mean values for precipitation, Evaporation, PmE, corrected precipitation ($\overline{P_C}$), corrected PmE ($\overline{P_CmE}$) and ($\overline{P_C}+\overline{R}-\overline{E}$). The last column shows the values for the alpha coefficients calculated by using equation (1).

The same procedure is then applied to the remaining four streams but, in this case, the derived pseudo-climatology precipitation is used in place of the GPCP climatology. The results are again shown in Table 1. With the applied precipitation corrections, the water balance, ($\overline{P_C}+\overline{R}-\overline{E}$), turns out to be well closed, that is its value is less than 1% of the precipitation and evaporation values (the dominant terms in the balance). The sole exception is the 1973-1978 stream which, however, is affected by both errors in the precipitation at latitudes poleward of ±30° and in the evaporation field.

3 Summary

A method to correct the excessive tropical precipitation over the oceans in the ERA-40 reanalysis has been presented. The basic idea of this method is the closure of the water budget. To this end, the assumption was made that the evaporation field is only affected by second order errors, hence for our purposes the evaporation is error-free.

The precipitation correction is only applied as a function of latitude and is different for each of the five periods in which the ERA-40 production phase was performed. The calculated correction coefficients are available from the authors.

Acknowledgments Author AT has been supported by the European Union project ENACT (EVK2-2001-00077) whereas author PK has been partially supported by the European Union project ERA-40 (EVK2-CT-1999-00027). The authors wish to thank David Anderson, Magdalena Balmaseda, Adrian Simmons, Tim Stockdale and Sakari Uppala for fruitful discussions.

References Huffman, G. J., Adler, R. F., Arkin, P., Chang, A., Ferraro, R., Gruber, A., Janowiak, J., McNab, A., Rudolf, B., and U. Schneider, U.: 1997, The Global Precipitation Climatology Project (GPCP) combined precipitation data set, *Bull. Am. Meteorol. Soc.*, **78**, 5–20 (incl. cover).

Quantifying relationships between rainfall and synoptic activity in the Australian region

Richard Wardle, Ian Simmonds and Kevin Keay

School of Earth Sciences
The University of Melbourne
Victoria, Australia, 3010
Email: *rwardle@unimelb.edu.au*

Differences in past climate regimes have primarily been associated with changes to the pole-to-equator temperature gradient (Budyko and Izrael, 1991). Changing the pole-to-equator temperature gradient could significantly alter the eddy fluxes, such as heat and moisture fluxes, that are associated with mid-latitude synoptic activity in the atmosphere (Lindzen, 1994).

Here we investigate the extent to which interannual variations in synoptic activity in the southeast of Australia are related to the interannual variations in rainfall. The climate of Australia is characterized by low annual mean rainfall and high rainfall variability making it sensitive to small changes in rainfall. Cyclone statistics for the southern hemisphere are generated by the Melbourne University vortex tracking scheme (Simmonds *et al.*, 1999) from the NCEP-NCAR Reanalysis dataset (Kalnay *et al.*, 1996). Four properties of the cyclones are presented here, namely the mean system density, the mean radius of systems and two measures of the 'strength' of the cyclones; the 'intensity' (Laplacian of the pressure at the center of the system) and the mean 'depth', which is proportional to the intensity times the radius squared (the area). Annual mean southeast Australian rainfall is computed from the Jones and Weymouth (1997) Australian precipitation dataset.

In Figure 1, we plot the correlation of the first differences of the time series of annual southeast Australian rainfall with the first differences of the four cyclone characteristics, for the period 1958-1997. All correlations are performed with the first differences of the time series to remove the effect of any trends. Shading in Figure 1 indicates regions where the correlation differs significantly from zero at the 95% confidence level. In Figure 1a, there is little significant correlation between the rainfall and the number of systems. In Figure 1b, the rainfall is positively correlated with the Laplacian of pressure in the vicinity of the southeastern region. The distribution of correlations with radius suggest a positive correlation over much of southern Australia and the Southern Ocean north of about 45^{o}S, with significant negative correlations to the south of this latitude (Figure 1c). This pattern is also pronounced in the correlations with the depth (Figure 1d). The distributions shown in Figure 1 suggest that the high rainfall is associated with systems with larger radii displaced to the north.

It is clear from Figure 1 that all aspects of cyclonic systems must be considered to build a more complete picture of the climate state. The net effect of the cyclones cannot simply be thought of in terms of their frequency, their size and intensity are also very important. Moreover, any future changes to the pole-to-equator temperature gradient and hence, the characterisitcs of synoptic systems (such as the radii), could profoundly impact other climate parameters, such as rainfall, in southeastern Australia, where the synoptic systems play an important climatic role.

Budyko, M.I., and Y.A. Izrael, 1991: In *Anthropogenic Climate Change*, ed. M.I. Budyko and Y.A. Izrael, pp. 277-318. Tuscon: Univ. Arizona Press.

Jones, D. and G. Weymouth, 1997: An Australian monthly rainfall dataset. Technical Report No. 70, Bureau of Meteorology, 19pp.

Kalnay, E., and Co-authors, 1996: The NCEP-NCAR Reanalysis Project. *Bull. Amer. Meteorol. Soc.*, 77, 437-471.

Lindzen, R.S., 1994: Climate dynamics and global change. *Ann. Rev. Fluid Mech.*, 26, 353-378.

Simmonds, I., R.J., Murray, and R.M. Leighton, 1999: A refinement of cyclone tracking methods with data from FROST. *Aust. Meteor. Mag.*, Special Issue, 35-49.

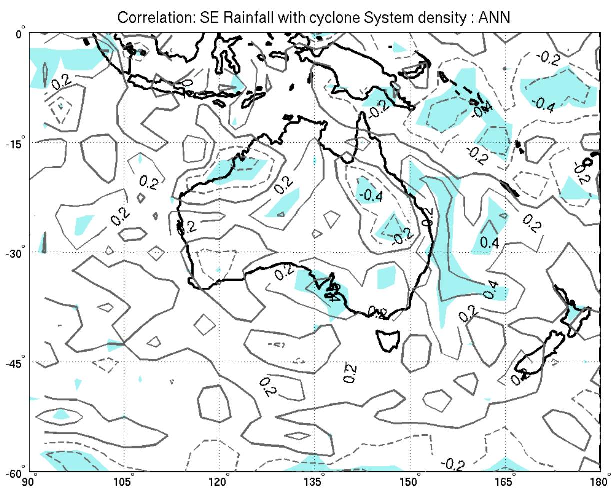

(a) Mean system density

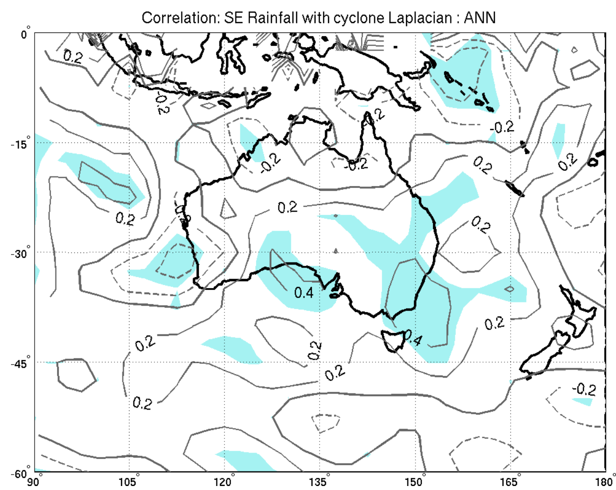

(b) Mean Laplacian of pressure

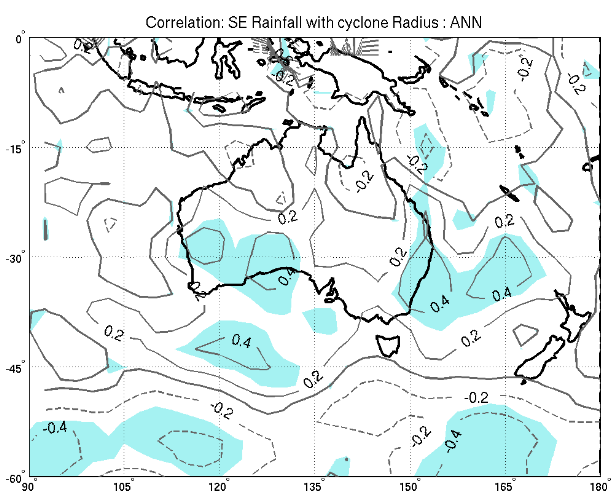

(c) Mean system radius

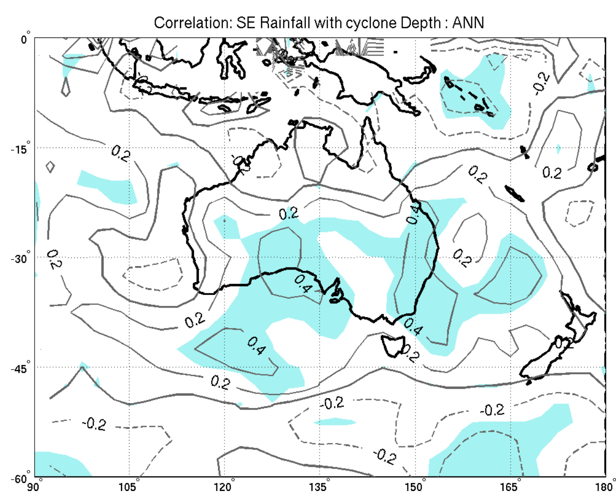

(d) Mean system depth

Figure 1: Correlation of the first differences of the annual time series of southeast Australian rainfall and the first differences of annual mean (a) system density, (b) Laplacian of pressure, (c) system radius and (d) system depth. The contour interval is 0.2. Statistical significance at the 95% confidence level is shaded.